RERTR 2009 — 31st INTERNATIONAL MEETING ON
REDUCED ENRICHMENT FOR RESEARCH AND TEST REACTORS

November 1-5, 2009
Kempinski Hotel Beijing Lufthansa Center
Beijing, China

TEM INVESTIGATION OF IRRADIATED ATOMISED AND GROUND U(MO) DISPERSION FUEL, WITH OR WITHOUT SI ADDED TO THE MATRIX

W. VAN RENTERGHEM, A. LEENAERS, S. VAN DEN BERGHE,
SCK•CEN, Nuclear Materials Science Institute, Boeretang 200, B-2400 Mol - Belgium.

M.-C. ANSELMET, F. CHAROLLAIS
CEA-Cadarache, DEN/DEC, 13108 St Paul Lez Durance Cedex – France

P. LEMOINE
CEA-Saclay, DEN/DISN, 91191 Gif sur Yvette Cedex – France

W. PETRY
Technische Universität München, Forschungsneutronenquelle Heinz Maier-Leibnitz (FRM II)
Lichtenbergstraße 1, 85747 Garching – Germany

ABSTRACT

The results of a transmission electron microscopy investigation of atomised and ground U(Mo) dispersion fuel in an aluminum matrix, with and without the addition of silicon, irradiated in the OSIRIS reactor in the framework of the IRIS-3 and IRIS-TUM irradiation programs, are discussed. The effect of the addition of Si and the different production methods on the fuel behavior, as revealed by optical microscopy, scanning electron microscopy and electron probe microanalysis, were reported previously. Also the TEM investigation reported here reveals small differences in the structure of the amorphous interaction layer, the matrix and the fuel kernels.

1. Introduction

To limit the civil use of high-enriched fuels, attempts are being made to replace the low-density UAl_x based dispersion fuels with high-density alternatives. The γ-U(Mo) alloy is momentarily considered as a promising candidate [1]. Past irradiation and PIE campaigns (e.g. IRIS-2 and FUTURE [2]), however, proved that the classical atomised U(Mo) dispersion fuel is not stable under irradiation conditions required for normal operation of plate-type fuel. The main cause for the instability was identified to be the irradiation behaviour of the U(Mo)-Al interaction phase which is formed between the U(Mo) particles and the pure aluminium matrix during irradiation [2,3]. TEM investigations have shown that this layer is amorphous and whereas in the fuel kernels the fission gas was retained in small bubbles forming a regular lattice

in the fuel kernels, no gas bubbles could be observed in the interaction layer [4]. The poor fission gas retention of the interaction layer caused large pores to develop between the interaction layer and the matrix aluminium, which eventually led to gross swelling and pillowing of the fuel plates.

Several attempts are being made to improve the stability of the U(Mo) dispersion fuel. One attempt is the addition of a small amount of Si to the Al matrix [5]. Even though the role of Si is not fully clarified yet, it was found that Si reduces the width of the interaction layer at the locations where there was close contact between the U(Mo) fuel and a silicon particle in the matrix at the beginning of irradiation or where a Si rich layer is formed around a fuel particle during production [6-8]. First irradiation experiments indeed show a reduction of the plate swelling and irradiation to a higher burn-up is possible.

Besides the use of atomised kernels, it is also possible to use ground U(Mo) kernels dispersed in an Al matrix. Ground fuel behaves somewhat differently under irradiation than atomised fuel, although the overall irradiation behaviour shows the same trends [9]. One possible effect of the difference in initial microstructure, observed by SEM, is the precipitation of fission gas bubbles on the grain boundaries in ground fuel at relatively low burnup [7]. Also in ground fuel, the addition of Si to the Al matrix reduces the thickness of the interaction layer where there was a contact between a Si particle in the matrix and the fuel kernel at the beginning of irradiation [7].

In this paper, the microstructural features of atomised U(Mo) fuel dispersed in a Al+2.1wt%Si matrix and of ground fuel dispersed in both a pure Al and an Al+2.1wt%Si matrix were characterized using transmission electron microscopy (TEM).

2. Experimental

AG3NE clad fuel plates containing atomised U(Mo) powder dispersed in an Al-2.1wt%Si matrix and AlFeNi clad fuel plates containing ground U(Mo) powder dispersed in either a pure Al or an Al-2.1wt%Si matrix, have been irradiated in the OSIRIS reactor between 09/2005 and 03/2007, in the framework of, respectively, the IRIS-3 and IRIS-TUM irradiation programs [9,10]. The fabrication data and irradiation history of the three plates are given in table 1.

The atomised fuel plate (U7MV8021) has a loading of ~8 g U_{tot}/cm^3 and an uranium enrichment of 19.8% ^{235}U. The meat consists of atomised U7.3wt%Mo particles dispersed in an Al matrix to which 2.1wt%Si is added. The cladding is fabricated from an AG3NE Al-2.81wt%Mg alloy. The atomised fuel plate was kept in the reactor for 7 irradiation cycles with a cladding temperature of 83°C during which a maximum burn-up of 59.3% ^{235}U (4.1×10^{21} fissions/cm^3 UMo) was reached.

Fabrication data	IRIS-3	IRIS-TUM	IRIS-TUM
Plate number	U7MV8021	U8MV8002	U8MV8503
Cladding	AlMg	AlFeNi	AlFeNi
Fuel U(Mo)	Atomized	Ground	Ground
Loading g/cm^3	7.8-8.0	8.33	8.45
Enrichment %^{235}U	19.8	49.2	49.5
Wt% Mo in U(Mo)	7.3	8.1	8.1
Matrix	Al+2.1wt% Si	Al (A5)	Al+2.1wt% Si
Meat Porosity (a.f.) (%)	2.2	7.9	8.9
Irradiation history			
Full power days	130.6	90.6	90.6
Temperature	83°C	96°C	97°C
Burn-up :			
Plate average (% ^{235}U)	48.8	14.6	14.1
Plate maximum (% ^{235}U) (LEU equivalent %^{235}U)	59.3	22.5 (56.3)	23.1 (57.8)
Fission density			
Plate average (f/cm^3 UMo)	3.4×10^{21}	2.4×10^{21}	2.4×10^{21}
Plate max (f/cm^3 UMo)	4.1×10^{21}	3.8×10^{21}	3.9×10^{21}

Table 1. Fabrication specifications and irradiation history of the fuel plates submitted for PIE at SCK•CEN.

The ground fuel plates have a comparable loading of ~8.4 g U_{tot}/cm^3, but a higher uranium enrichment of approximately 49.5% ^{235}U to reach more severe irradiation conditions. The meat of the fuel plates consists of ground U8.1wt%Mo particles dispersed in either a pure (A5) aluminum matrix (plate U8MV8002) or an Al matrix to which 2.1 wt% Si (U8MV8503) is added. The cladding of the fuel plates is an Al alloy with 1% Fe, 1% Ni and 1% Mg, commonly called AlFeNi. The ground fuel plates were kept in the reactor during 5 irradiation cycles at a temperature of around 97°C. At their end of life, the plates have a maximum burn-up of respectively 22.5% ^{235}U (56.3% ^{235}U LEU equivalent, 3.8×10^{21} fissions/cm^3 UMo) for plate U8MV8002 and 23.1% ^{235}U (57.8% ^{235}U LEU equivalent, 3.9×10^{21} fissions/cm^3 UMo) for plate U8MV8503. It should be noted that despite the different enrichments and irradiation conditions, the LEU equivalent burn-up at plate maximum of the three plates is comparable.

After unloading and non destructive characterization at the CEA site, samples were cut at the maximum flux plane, embedded using a stainless steel envelope to limit the forces during cutting and sectioned. From each specimen, four sections were cut (see [7] for the cutting scheme). Three of these sections were used for the OM, SEM and EPMA analysis reported previously [7]. The smaller spare sections were used to prepare the TEM specimens. From each section, a thin slice of about 0.3 mm thick was cut in cross-section. After cutting, the stainless steel envelope was removed and the thin slices were mechanically polished to reduce the thickness to about 100 µm. Each thin slice was cut in two halves to reduce the length of the slice below 3 mm. Next, the specimens were glued on a golden grid with an aperture 0.6 mm using M-Bond 610 glue and electrochemically polished until perforation. To improve the specimen quality, the specimen preparation was finished with ion beam milling.

After electrochemical polishing, the specimens were analysed in a JEOL 6310 SEM to verify if the fuel, the interaction layer and the aluminum matrix, are present at the edges of a hole. The ion beam milling did not significantly alter the shape of the hole. Afterwards, the

specimens were investigated with a JEOL 3010 transmission microscope operating at 300kV. Conventional dark field and bright field images were used. The crystal structures of the different phase were characterized using electron diffraction and compared with the ICSD data base. High-resolution images (HRTEM) were recorded to visualize the local crystal structure.

3. Results

3.1 Fuel plate U7MV8021

The SEM image of figure 1 shows the specimen after electrochemical polishing. The hole is formed in the meat of the specimen. It can be observed that both the fuel kernel and the interaction layer are present at the border of the hole, but the Al(Si) matrix is not.

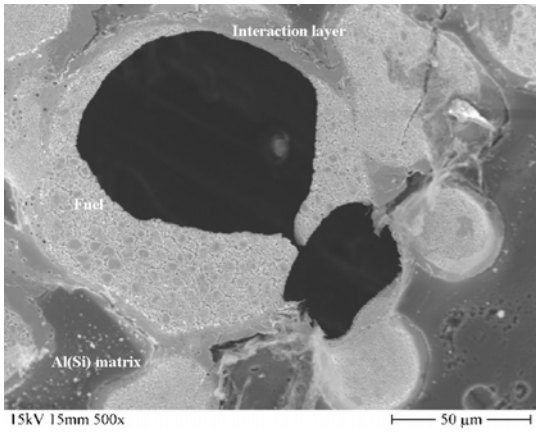

Figure 1. SEM image of specimen U7MV8021 showing the holes formed during electrochemical polishing. The interaction layer and the fuel kernel border at the hole, but the Al matrix does not.

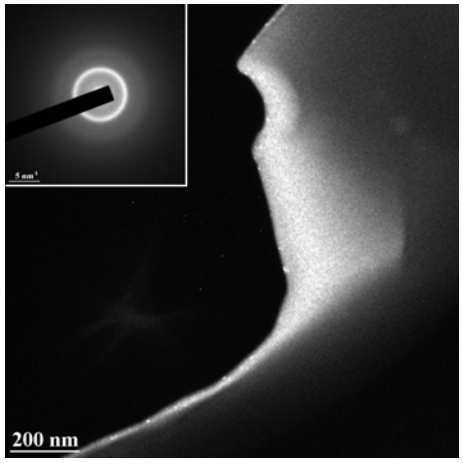

Figure 2. Dark field image with the corresponding diffraction pattern in the inset showing the amorphous nature of the interaction layer in specimen U7MV8021.

The nature of the interaction layer is shown in figure 2. The dark field image shows no distinct features and in the diffraction pattern, only a diffuse diffraction ring is visible. Both images prove the amorphous nature of the interaction layer. The diameter of the diffuse ring is a measure for the nearest neighbour distance. In this specimen, this distance is 0.25 nm.

The dark field image of figure 3a shows that fission gas bubbles are formed in the U(Mo) grains of the fuel. Similar to what is found in the FUTURE atomized fuel specimen in the pure Al matrix [2] and the RERTR-6 plate R2R010 [11], the fission gas bubbles are lying on a regular lattice. The diffraction pattern of figure 3b shows that the specimen is oriented along the [33-1] zone axis. The inset of figure 3b shows an enlarged image of the transmitted beam. Superstructure reflections were observed, related to the lattice of the fission gas bubbles. The exact symmetry of the fission gas bubble lattice cannot be determined from this image alone, but it is clear that both lattices are not fully coincident. There is a set of planes of the bubble lattice, which is parallel to the (1-10) plane of the U(Mo), but no planes in the bubble lattice were found to be parallel to the (103) or (013) planes. On the other hand, the planes with the largest interplanar distance in the bubble lattice were not found to be parallel to a plane in the U(Mo) grain. For the fission gas bubble lattice, it was measured that the average bubble size is 2 nm and the lattice parameter is 7 nm.

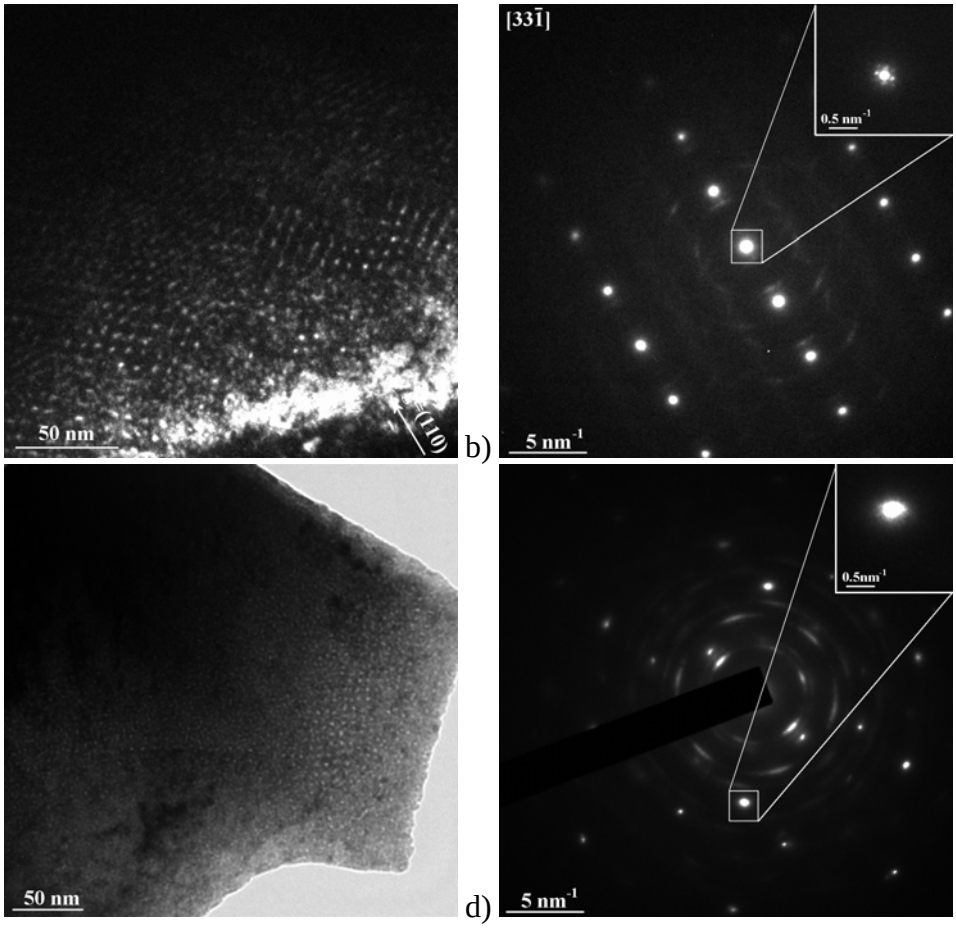

Figure 3. a) Dark field image showing fission gas bubbles organised on a regular lattice in specimen U7MV8021. b) The corresponding diffraction pattern. The inset shows an enlarged view of the reflection in the white rectangle, in which superlattice reflections, clearly separated from the main reflection, can be observed. c) Out of focus bright field image showing an area where the fission gas bubbles are barely aligned on a regular lattice. d) The corresponding diffraction pattern in which no clearly separated superstructure reflections were found.

Not all fission gas bubbles form a regular lattice. Figure 3c is a bright field image of another area of the fuel kernel recorded in out of focus conditions to show the fission gas bubbles. Even though the fission gas bubbles tend to align in the interior of the grain, no entirely regular lattice is formed there. Moreover, no ordering is occurring near the edges of the grain. Also in the corresponding diffraction pattern of figure 3d, no clear superstructure reflections were observed in this area.

3.2 Fuel plate U8MV8002

The location of the holes formed during electrochemical polishing was verified with SEM and the result is shown in figure 4. All holes are formed in the meat part of the fuel plate, while the cladding remained intact. Several holes were formed during the polishing at different locations in the specimen. In this specimen, all three different phases, the Al matrix, the interaction layer and the fuel kernel, are present at the edges of the hole.

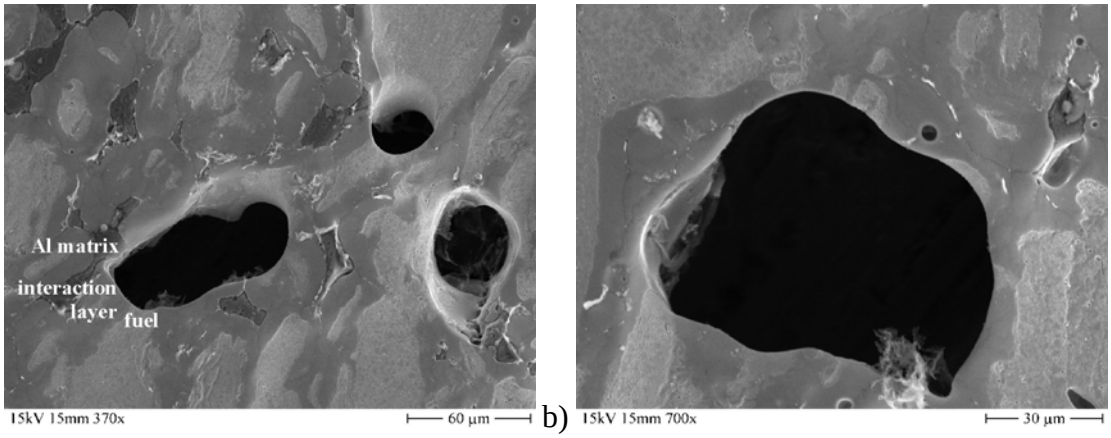

a) b)

Figure 4. a and b) SEM images of specimen U8MV8002 showing the holes formed during electrochemical polishing. The Al matrix, the interaction layer as well as the fuel kernel border at the hole.

Figure 5a shows a dark field image of the Aluminium matrix. In this specimen, no Si is added to the matrix and it consists of pure Al. The corresponding diffraction pattern allowed to identify this area as crystalline Al. No amorphisation or other phase changes were found and only typical radiation induced defects can be observed in this image. The main type of dislocation loops in crystals with a face centred cubic crystal structure are Frank loops. The sharp line contrast indicated by the letter F in figure 5a is the typical contrast of a Frank loop when viewed edge on and agrees with the orientation of the crystal. The dark round spots indicated by the letter D in figure 5a are also radiation induced dislocation loops. These loops were not analysed in detail, but they probably are Frank loops as well.

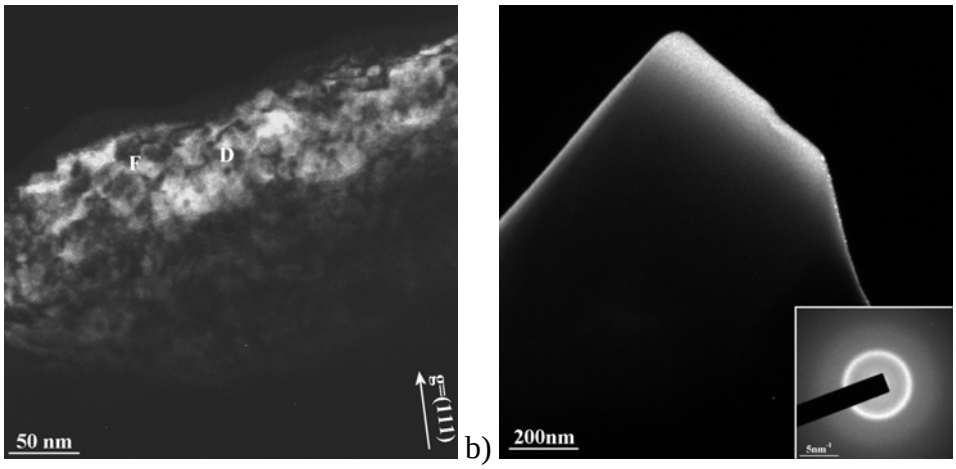

a) b)

Figure 5. a) Dark field image of the Al matrix in specimen U8MV8002 showing radiation induced defects. b) Dark field image of the amorphous interaction layer. The inset shows the corresponding diffraction pattern proving the amorphous character of the interaction layer.

A few transparent areas were found, which, in combination with the SEM images, can be attributed to the interaction layer. A dark field image and the corresponding diffraction pattern of such an area are shown in figure 5b. In the diffraction pattern in the inset, only a diffuse diffraction intensity was found which is typical for an amorphous material. In a dark field image, obtained by selecting a small section of the diffuse diffraction ring, no features can be distinguished, confirming that the

interaction layer is amorphous. Taking the most intense part of the diffuse ring as a measure for the nearest neighbour distance, a value of 0.24 nm is obtained.

Even though similar featureless dark field images were obtained on most other transparent areas in the interaction layer, indicating that it is entirely amorphous, locally small crystalline grains were found as well. The bright field image of figure 6a, shows an example of such a crystalline part. The diffraction contrast in the image already indicates a crystalline structure and the sharp reflections in the corresponding diffraction pattern, shown in the inset, confirm the crystalline nature. However the complexity of the pattern shows that the selected area is not a single crystal. Reflections from multiple grains with different orientations can be recognized, but the number of grains is too low to form complete diffraction rings. To reveal the crystal structure in the complex diffraction pattern, a few circles were manually drawn on the image, which coincide with the most intense reflections. It can be observed that all intense reflections lie on one of these circles. When calculating the interplanar distance corresponding with each of the circles, it was found that they all correspond with lattice planes of an UAl_3 crystal structure.

A confirmation of the conclusions from the diffraction pattern was found in the high resolution image of figure 6b, with the Fourier transform of the image in the inset. The largest distance between the planes, both measured from the real image and the Fourier transform, was 0.430 nm which corresponds with the (100) planes of UAl_3. The angle between these planes is 90°. These observations correspond with an UAl_3 crystal structure oriented along the [100] zone.

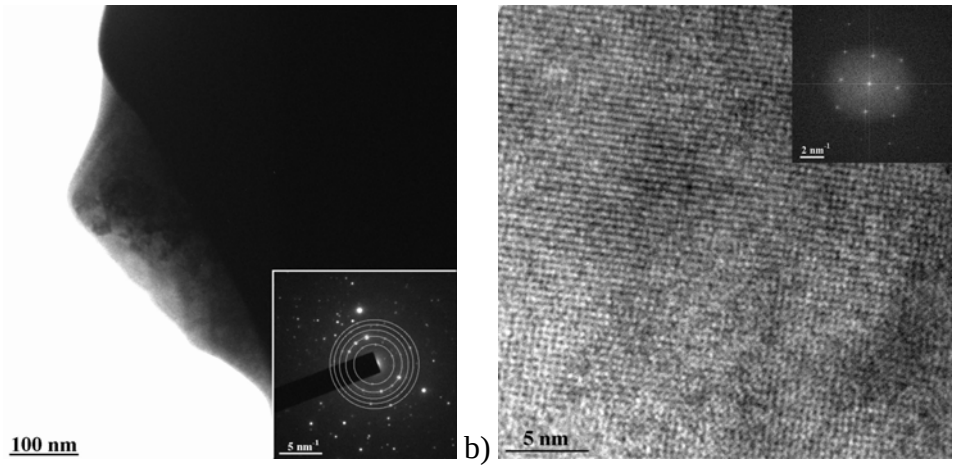

Figure 6. a) Bright field image of a crystalline grain in the interaction layer in specimen U8MV8002. The inset depicts the corresponding diffraction where the rings correspond with the locations of the diffraction spots of a UAl_3 –type structure. b) High-resolution image confirming the UAl_3 crystal structure, the inset shows the Fourier transform of the high-resolution image.

a) 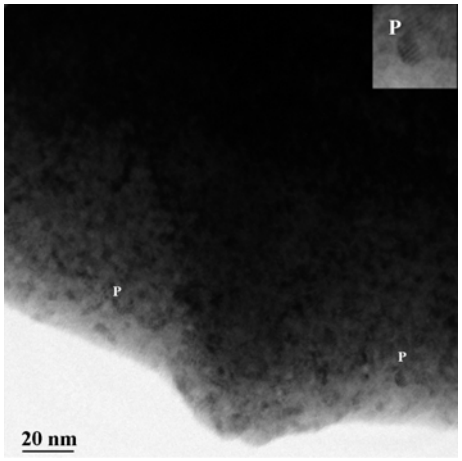

b) 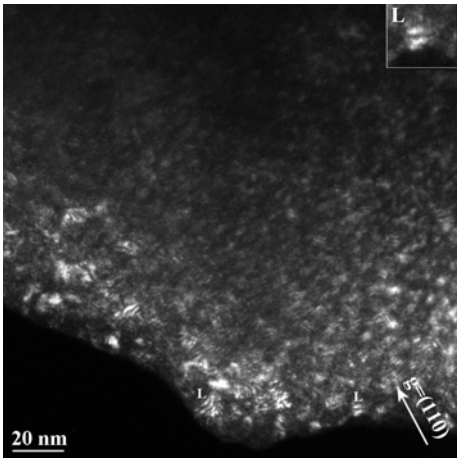

Figure 7. a) Bright field image showing the defect structure of the U(Mo) grain. The inset shows an enlarged image of the Moiré pattern caused by an UO_2 particle. b) The corresponding dark field image. Here, the inset shows an enlarged view of the double lobe contrast typical of a dislocation loop.

In the U(Mo) grains which are present at the edges of the holes, only a few transparent areas could be found. During the grinding of the fuel, a large amount of stress is applied to the U(Mo) metal. It can therefore be expected that a large number of defects, and dislocations in particular, will be present in the U(Mo) grains. Figure 7 shows an in-focus bright and dark field image. The Moiré patterns in the bright field image, like the ones indicated by the letter P and shown in the inset of figure 7a, result again from the small UO_2 particles. Furthermore, a double lobe contrast, as indicated by an L and shown in the inset in figure 7b, which is typical for dislocation loops, is present as well. On the other hand, no line dislocations or any other defect resulting from high stresses can be observed in these images.

Figure 8a shows a bright field image of the same grain under out-of-focus conditions to clearly reveal the presence of gas bubbles. It was observed that many small fission gas bubbles are present in the U(Mo) grains and that they form a regular lattice. The average size of the bubbles measured in the bright field image equals 2 nm and the lattice parameter is 7nm.

The corresponding diffraction pattern in figure 8b gives additional information about the U(Mo) grain. The sharp intense spots all agree with the crystal structure of U(Mo) for a grain oriented along the [1-10] axis. Apart from the intense reflection, weaker diffraction rings can be observed, which agree with an UO_2 crystal structure. Due to the exposure to air during the sample preparation and handling, the uranium oxidises and many small oxide grains were formed. The diffraction intensity within one ring is not equally distributed, but a higher intensity is observed near diffraction spots of the U(Mo) matrix. There is no exact epitaxial relation, but there is a preference for the oxide to align with the U(Mo) matrix.

The inset in figure 8b shows the diffraction pattern around the transmitted beam, recorded at a longer camera length. The small satellite reflections around the transmitted beam correspond with the diffraction at the fission gas bubble lattice. From the few diffraction spots, an estimation of the bubble lattice parameters can be obtained, but too few data are available to fully characterise its structure.

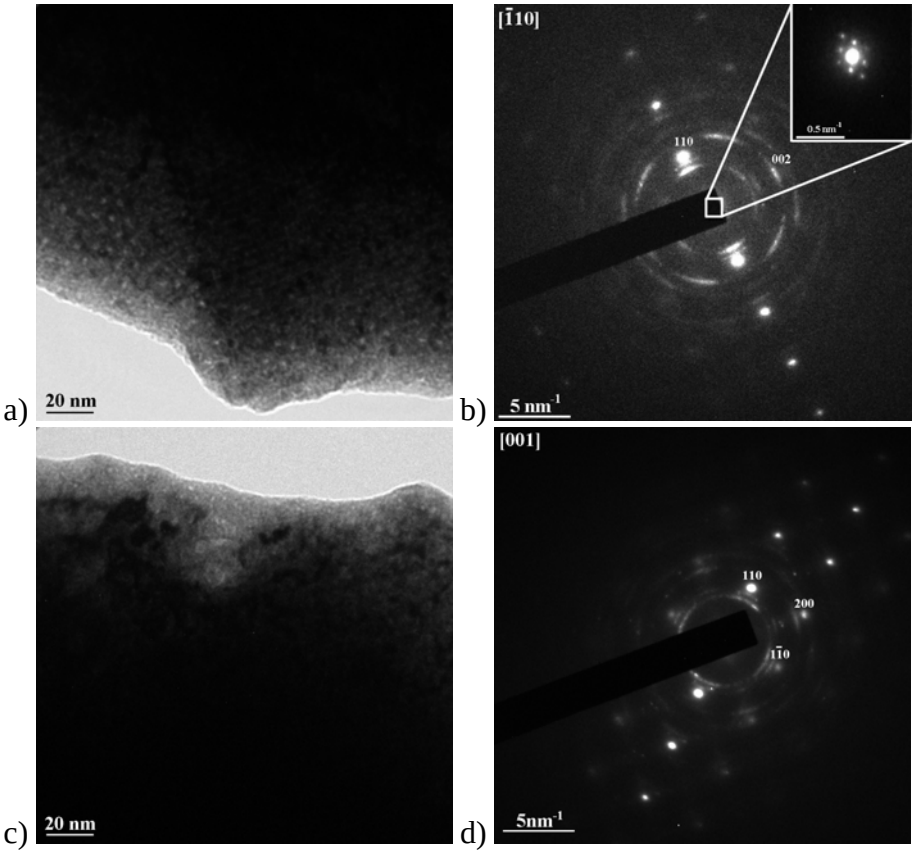

Figure 8. a) Out-of-focus bright field images showing the U(Mo) grain containing a fission gas bubble lattice. b) The corresponding diffraction pattern. The inset shows an enlarged image of the transmitted beam. The small satellite spots are the result of diffraction at the bubble lattice. c) Out-of-focus bright field image and d) the corresponding diffraction pattern of an U(Mo) grain that does not contain a regular fission gas bubble lattice.

There is an orientation relation between the bubble lattice and the underlying U(Mo) matrix. All planes of the bubble lattice are parallel to the planes of the U(Mo). However, the planes with the largest distance in the U(Mo) do not correspond with the planes with the largest distance in the bubble lattice. In figure 8b, the bubble lattice reflection which is parallel to the (110) reflection of the U(Mo) is not the one closest to the transmitted beam and hence its interplanar distance is not the largest one of the bubble lattice. More research, involving the examination of larger transparent areas is required to fully characterise the bubble lattice.

Also in this sample, the bubble lattice was not observed in all U(Mo) grains. Figures 8c and 8d show an out-of-focus bright field image and the corresponding diffraction pattern of such an U(Mo) grain. The diffraction pattern confirms the presence of U(Mo) and shows that the grain is oriented along the [001] zone. The diffuse ring pattern of small UO_2 particles is present as well. However, no superstructure reflections were observed. However, the bright field image of figure 8c indicates that also here gas bubbles were formed, but contrary to the grain of figure 8a, these bubbles do not form a regular lattice. Moreover, only bubbles can be observed close to the edge of the specimen, not in the bulk. Therefore, it must be stipulated that it cannot be excluded that the features observed at this location are not bubbles formed by fission gas, but artefacts resulting from the ion beam specimen preparation.

3.3 Fuel plate U8MV8503

The overview SEM image of the specimen from fuel plate U8MV8503 is shown in figure 9a. During the electrochemical polishing, the cladding on one side broke off. Moreover, in the upper part of the meat, large holes were found, indicating that part of the fuel fell out. Even though, the specimen does not appear to be intact anymore, it is still sufficiently supported to allow the TEM investigation. Figure 9b shows a SEM image of a few of the electrochemically polished holes of the second specimen. The image shows that all three phases are present at the edges of the holes, even if they are not all around the same hole.

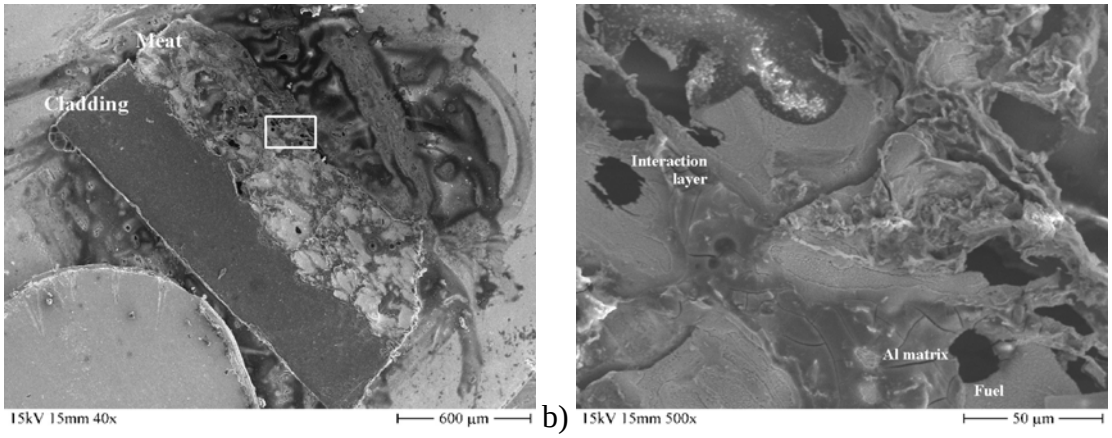

a) b)

Figure 9. a) SEM image showing the location of the holes in specimen U8MV8503. b) Detailed SEM image of the area inside the rectangle of a) showing a few holes formed during electrochemical polishing, where the different phases are indicated.

A dark field image of the Al(Si) matrix is shown in figure 10a. Very few transparent areas were found in the matrix and the contrast in the image, like the irregular edge of the bright area or the fringe contrast, can be largely attributed to an imperfect specimen preparation. However, the microstructural features, which were reported for specimen U8MV8002, can be recognised in this specimen as well. The matrix remained crystalline during irradiation and the typical radiation induced dislocation loops can be recognised in the image. In figure 10a, two of these defects are indicated with the letter D.

Figure 10b shows the general aspects of the interaction layer. At almost all areas that were observed, it was found that the interaction layer is again amorphous. The dark field image in figure 10b, shows the featureless character of the interaction layer and the diffraction pattern in the inset shows a diffuse intensity which proves the absence of a periodic structure. Similar to the previous specimens, the more intense band corresponds with the nearest neighbour distance in the amorphous material. The diameter of the ring translates to a distance of 0.25 nm. In view of the width of the ring, this value does not differ significantly from the value measured in other specimens.

a) 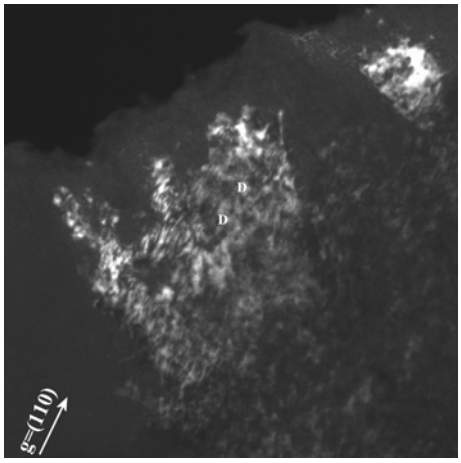

b) 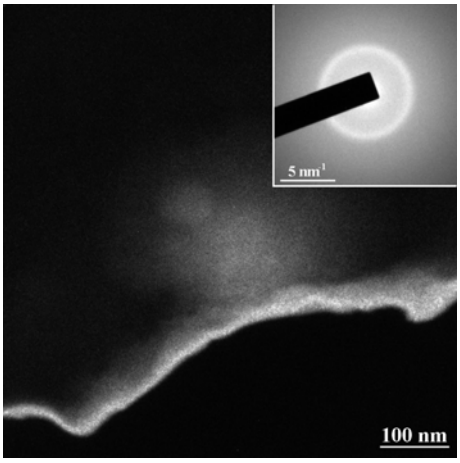

Figure 10. a) Dark field image of the Al(Si) matrix of specimen U8MV8503. The D indicates two examples of radiation induced dislocation loops. b) Dark field image of the interaction layer. The corresponding diffraction pattern in the inset shows the amorphous nature.

Also in this specimen, a location was found in the interaction layer that was not amorphous. The bright field image in figure 11a shows that this part of the interaction layer does not show a featureless contrast and the diffraction pattern in the inset shows sharp crystalline reflections. It was not possible to completely identify the phase from the diffraction pattern. Two different reflections corresponding with a planar distance of 0.34 nm can be clearly seen in the diffraction pattern, but none of the expected phases has planes with this distance. The other reflections in the diffraction pattern agree with the UAl_3 phase.

a) 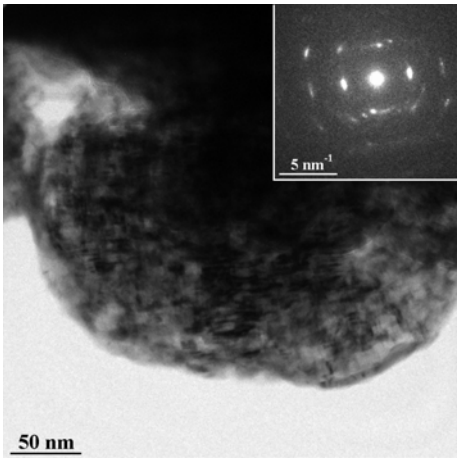

b) 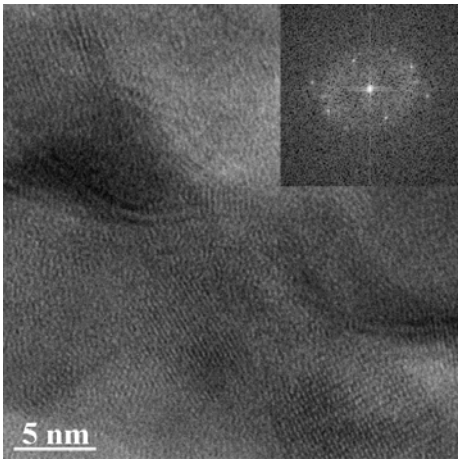

Figure 11. a) Bright field image of a crystalline part of the interaction layer with the corresponding diffraction pattern in the inset. b) A HRTEM image indicating the presence of the UAl_3 phase.

A further confirmation of the UAl_3 phase can be found in the high-resolution image of figure 11b. From both the direct image and the Fourier transform given in the inset, it can be calculated that the crystal structure contains lattice distances of 0.4 nm and 0.3 nm, in agreement with the (100) and (011) planes of UAl_3. Both planes make an angle of 90°, as observed in the HRTEM image. An UAl_3 grain oriented along the [01-1] zone axis would generate a similar high-resolution image. It was noted that the

grain was not stable under the electron beam. Especially when the electron beam was focused for the HRTEM image, it was observed that the area under the electron beam became amorphous.

An example of the structure of an U(Mo) grain and the corresponding diffraction pattern are shown in figure 12. In the diffraction pattern, sharp diffraction spots are present, which correspond to different lattice planes of the U(Mo) crystal structure. From the diffraction pattern, it was calculated that the grain is oriented along the [1-33] zone. Apart from the sharp spots, a few weaker diffraction rings can be observed as well, corresponding with an UO_2 crystal structure. Because the intensities of these rings are much weaker than the diffraction spots, the contribution to the TEM-images is limited.

The contrast in the dark field image of figure 12a is dominated by an ordered structure of gas bubbles or voids. A few transparent areas were found in different U(Mo) grains and at all locations, a bubble lattice is observed. This observation is similar to fuel plate U8MV8002. The size of the bubbles is about 3 nm and they are separated by a distance of 6 nm.

The inset in the diffraction pattern of figure 12b shows that weaker satellite spots are present around each of the diffraction spots, resulting from a double diffraction of the electron beam. The locations of the satellite spots reflect the distance between bubble lattice planes and the orientation relation with the U(Mo) grain. It was measured that the distance between two bubble lattice planes is indeed about 6 nm. The lattice does not have exactly the same orientation as the U(Mo) grain. On the one hand, there is a satellite reflection parallel to the direction of the (110) reflection, but, on the other hand, no satellite was found in the directions parallel to either the (310) or (30-1) reflections, which would be required for an exact orientation agreement.

a) 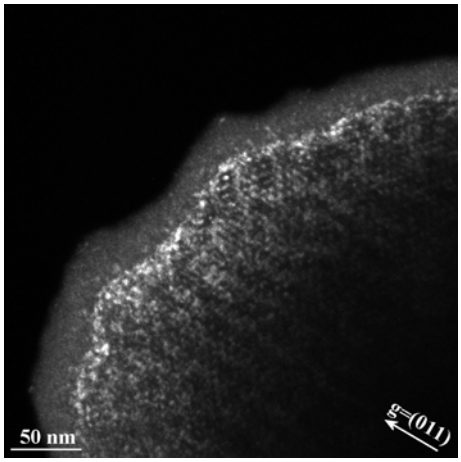

b) 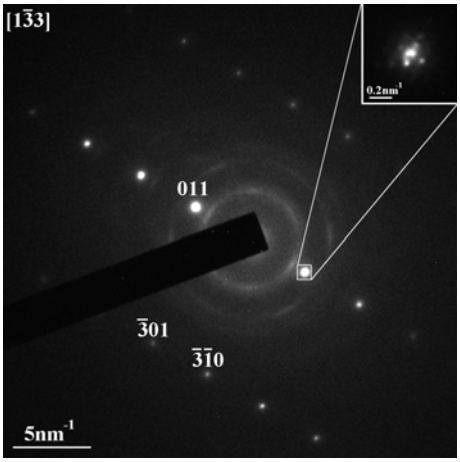

Figure 12. a) Dark field image of a U(Mo) fuel grain, showing a superlattice of fission gas bubbles. b) The corresponding diffraction pattern. The inset gives an enlarged image of the indicated diffraction spot. Superstructure reflections can be recognised which can be attributed to the gas bubble superlattice.

4. Discussion

4.1 The interaction layer

As the instability of the atomised U(Mo) fuel was attributed to the formation of an amorphous interaction layer, it was verified if the addition of Si to the Al matrix or the different microstructure of the ground fuel had an influence on the structure of the interaction layer. It was observed in the TEM-images that the largest part of the interaction layer is still completely amorphous and from the diffusion ring in the diffraction pattern, the nearest neighbour distance of the atoms was measured, resulting in values of 0.24 nm to 0.25 nm. These do not differ significantly from each other and are also comparable

with the measurement in the atomised fuel of the FUTURE irradiation [4]. No indications were found that the addition of Si to the Al matrix would have any effect on the interaction layer structure itself. Local interactions between Si particles in the matrix and the fuel kernels, as observed in the EPMA investigation [7], have unfortunately not been observed. It should be noted that those interactions were only observed when a Si particle was located close to a fuel kernel at the beginning of irradiation and occurred only locally. The SEM image of the TEM samples showed that no such location was found near the edges of the hole and consequently did not occur in the transparent areas of the specimens. In view of the low Si content of the matrix, it is not inconceivable that the dilution of the Si in the interaction layer is too high to have a significant overall effect.

In the atomised dispersion fuel, the interaction layer was amorphous at all observed locations. However, in both ground fuel specimens, small crystalline areas were found. From the present experiments, it could not always be fully identified which phase was formed, but the formation of UAl_3 was confirmed in specimen U8MV8002. In specimen U8MV8503, indications were found of UAl_3, but that phase was not stable under the electron beam. The occurrence of a crystalline interaction layer has been reported to occur in pin type U(Mo) fuel [12] and in heavy ion irradiated fuel [17]. It is known that temperature plays an important role in the crystallisation of the interaction phase. The pin type fuel temperature is higher during irradiation and the ion irradiations where at even higher temperatures. This can lead to a crystallisation of the interaction layer. The irradiation of the ground fuel was performed at a lower temperature, with an estimated fuel temperature of roughly 200°C, which is comparable to the previously investigated atomized dispersion fuel. It was observed by SEM that during irradiation almost all Al was consumed by the interaction layer [13]. Consequently, the thermal conductivity of the fuel is lowered and therefore, it is likely that the temperature of the fuel locally increased to a higher value than in the atomised fuel. The postulated higher temperature may offer an explanation for the formation of small crystalline areas in the interaction layer.

4.2 The U(Mo) fuel kernels

In the fuel kernels, fission gas bubbles were observed in underfocus bright field images. Areas were found in all three specimens, where the bubbles align on a regular lattice. A similar kind of bubble ordering was also observed previously in atomised U(Mo) fuel [4] and for He implantation in metals at a temperature of $0.2T_m$, the melting temperature [14]. It was shown that this lattice aligns with the lattice of the U(Mo) grain, but it does not have the exact same symmetry or orientation. For implantation experiments, it was reported that, in general, the He bubble lattice has the same symmetry as the metal, but it has been observed that regions can exist where the ordered bubble array has an orientation that is rational with, but different from, that of the crystal lattice of the host metal [15]. The exact crystal structure and orientation relation of the bubble lattice could not be determined in our case, because it would require larger and more numerous transparent regions. The distance between two gas bubbles is about 6.9 nm and the bubble size was measured to be around 2 nm in specimens U7MV8021 and U8MV8002 and 3 nm in specimen U8MV8503. In specimens U7MV8021 and U8MV8002 also U(Mo) grains were found which did not contain a fission gas bubble lattice. In specimen U8MV8503, no such areas were observed, but one can expect that they do exist.

These results can also be compared with the TEM results of the atomised U(Mo) dispersion fuel of the FUTURE irradiation [4]. In that fuel plate, a gas bubble lattice was found in all observed grains. The distance between the bubbles was measured to be 6-7 nm, which is comparable with the results on the current specimens, but the size was roughly 1-2 nm. Compared to the previous measurements, the bubble diameter therefore increased. The IRIS-3 and IRIS-TUM plates were irradiated to a higher burn-up compared to the FUTURE plates. Consequently, more fission gas is formed and, as the fission gas is

collected in these gas bubbles, the size increase of the bubbles could be expected. A similar observation was made by Gan et al. in higher burn-up fuel from the RERTR irradiations [11]. The fact that some grains did not contain a regular lattice anymore indicates that the bubble lattice can no longer accommodate all fission gas. In the case of helium implantation in Cu, Johnson et al. reported that with increasing He concentration, the bubble structure coarsens and the ordered bubble arrays are replaced by random arrays of larger bubbles [16]. Also, the higher defect concentrations expected in ground fuel may lead to areas where the bubble lattice cannot form due to the lattice stress, even if the TEM investigations have not revealed important concentrations of line defects.

Still a lot of information needs to be found on the fission gas bubble lattice. It is not known exactly yet what is the exact symmetry and lattice parameter of the bubble lattice and whether they are the same for all U(Mo) grains or if local differences can influence the lattice parameters, which is probable. Also the exact relation with the underlying U(Mo) lattice is not yet clear. It was found that at all locations the planes of the bubble lattice are parallel with the U(Mo) lattice planes, but planes with the largest distance in the bubble lattice do not correspond with the planes with the largest distance in the U(Mo) lattice. An improvement of the specimen preparation, leading to more, larger and thinner areas is required to correctly answer these questions.

5. Conclusions

One specimen of atomised U7.3wt%Mo fuel dispersed in an Al2.1wt%Si matrix from the irradiated fuel plate U7MV8021 and two specimens of ground U8.1wt%Mo fuel dispersed in an Al and an Al2.1wt%Si matrix from irradiated fuel plates U8MV8002 and U8MV8503 were investigated with TEM. Information was obtained about the crystallographic structure of the fuel kernel, the interaction layer and the Al matrix. The specimen preparation procedure is not optimal yet, but as confirmed by SEM images, transparent areas were found in all three phases.

The interaction layers around the U(Mo) fuel kernel were found to be mainly amorphous in all three specimens. The nearest neighbour distances were measured to be 0.24 nm to 0.25 nm. In the ground fuel specimens, locations were found in the interaction layers which contain crystalline phases. It was not possible to fully identify the crystalline phase in all cases, but the presence of the UAl_3 phase was confirmed in both specimens. No effect of the addition of Si to the matrix on the structure of the interaction layer could be demonstrated, which may be related to the low Si concentration used.

In all specimens, a fission gas bubble lattice was found in the U(Mo) grains. The distance between the bubbles is about 7 nm and the average bubble size was 2-3 nm. Apart from fuel plate U8MV8503, also grains were found which did not contain a bubble lattice. Small gas bubbles were observed there as well, but they are randomly dispersed. It is expected that the higher burn-up of these samples and the resulting higher gas concentrations are at the basis of this and that the nanobubble lattice is starting to break down in some locations.

The main effect of the irradiation on the Al matrix is the incorporation of radiation induced defects. Many dislocation loops were observed. Most of them are Frank-type loops, which is a typical radiation induced defect in crystals with a face centred cubic lattice.

6. References

[1] S.L. Hayes, M.K. Meyer, G.L. Hofman, R.V. Strain, in: Proceedings of the 21st International Meeting on Reduced Enrichment for Research and Test Reactors (RERTR), Sao Paulo, Brazil, 1998.

[2] A. Leenaers, S. Van den Berghe, E. Koonen, C. Jarousse, F. Huet, M. Trotabas, M. Boyard, S. Guillot, L. Sannen, M. Verwerft, J. Nucl.Mater. 335 (2004) 39.

[3] A. Leenaers, S. Van den Berghe, E. Koonen, C. Jarousse, F. Huet, M. Trotabas, M. Boyard, S. Guillot, L. Sannen, M. Verwerft, in: Proceedings of the 8th International Topical Meeting on Research Reactor Fuel Management (RRFM), Munich, Germany, 2004.
[4] S. Van den Berghe, W. Van Renterghem and A. Leenaers, J. Nucl. Mater. 375 (2008) 340.
[5] M. Ripert, S. Dubois, P. Boulcourt, S. Naury and P. Lemoine in: Proceedings of the 10th International Topical Meeting on Research Reactor Fuel Management (RRFM), Sofia, Bulgaria (2006).
[6] A. Leenaers, S. V. d. Berghe, S. Dubois, J. Noirot, M. Ripert and P. Lemoine in: Proceedings of the 12th International Topical Meeting on Research Reactor Fuel Management (RRFM), Hamburg, Germany (2008).
[7] A. Leenaers, S. Van den Berghe, M.-C. Anselmet, J. Noirot, P. Lemoine, A. Röhrmoser, W. Petry, Proceedings of the 30th international meeting on reduced enrichment for research and test reactors (RERTR), Washington, USA, (2008).
[8] D. D. Keiser, A. B. Robinson, D. E. Janney and J. F. Jue in: Proceedings of the 12th International Topical Meeting on Research Reactor Fuel Management (RRFM), Hamburg (Germany) (2008).
[9] W. Petry, A. Röhrmoser, P. Boulcourt, A.Chabre, S. Dubois, P. Lemoine, C. Jarousse, J. Falgoux, S. Van den Berghe and A. Leenaers in: Proceedings of the 12th International Topical Meeting on Research Reactor Fuel Management (RRFM), Hamburg (Germany) (2008).
[10] S. Dubois, J. Noirot, J. M. Gatt, M. Ripert, P. Lemoine and P. Boulcourt in: Proceedings of the 11th International Topical Meeting on Research Reactor Fuel Management (RRFM), Lyon, France (2007).
[11] J. Gan, D.D. Keiser, D.M. Wachs, A.B. Robinson, B.D. Miller and T.R. Allen in: Proceedings of the 13th International Topical Meeting on Research Reactor Fuel Management (RRFM),Vienna, Austria, (2009).
[12] K.T. Conlon, D.F. Sears, in: Proceedings of the 10th International Topical Meeting on Research Reactor Fuel Management (RRFM), Sofia, Bulgaria, 2006.
[13] M. Ripert, S. Dubois, J. Noirot, P. Boulcourt, P. Lemoine, S. Van den Berghe, A. Leenaers, A. Rohrmoser, W. Petry and C. Jarousse in: Proceedings of the 12th International Topical Meeting on Research Reactor Fuel Management (RRFM), Hamburg (Germany) (2008).
[14] P.B. Johnson, D.J. Mazey, J. Nucl. Mater. 218 (1995) 273.
[15] P.B. Johnson, F. Lawson, Nucl. Instr. Meth. Phys. Res. B 243 (2006) 325.
[16] P.B. Johnson, K.L. Reader, R.W. Thomson, J. Nucl. Mater. 231 (1996) 92.
[17] N. Wieschalla, A. Bergmaier, F. Böni, K. Böning, G. Dollinger, R. Grossmann, W. Petry, A. Röhrmoser, J. Schneider, J. Nucl. Mater., 357, (2006), 191-197.